nature climate change

Article https://doi.org/10.1038/s41558-026-02599-9

More eddying of subtropical western boundary currents boosts stratification and cools shelf seas

Received: 23 September 2025

Accepted: 23 February 2026

Published online: 15 April 2026

Check for updates

K. L. Gunn [1] & L. M. Beal [2]

Ocean eddies are intensifying with climate change, especially in western boundary currents. Boundary currents separate coastal seas from the open ocean, but eddies drive cross-slope fluxes that can adjust the current and change shelf-sea conditions. Here we analyse two years of mooring observations in the Agulhas Current, diagnosing eddy dynamics and fluxes. We find that eddies converge heat and salt towards the current core over time, cooling adjacent shelf seas while broadening and stratifying the current. On the inshore edge, frequent 10-km frontal instabilities dominate, pumping cold, nutrient-rich waters up onto the shelf, while farther offshore 100-km meanders move heat onshore. The result is accelerated warming at the surface, but cooling at depth. Similar tendencies are expected in all subtropical western boundary currents as eddying increases, implying that adjacent shelf and slope seas will bear more extremes in the future, even while the strength of these currents may hold steady.

Evidence is growing that the ocean is eddying more with climate change and that western boundary currents are a hotspot for this change[1–8]. Western boundary currents carry heat poleward as part of the global climate conveyor and coupling with the overlying atmosphere drives weather extremes over mid-latitude land masses further downstream[9,10]. Rapid warming of these currents, observed from space, has been linked to increasing continental storms, rainfall and heat extremes, with the Agulhas Current implicated in rising summer heat and rainfall over southern Africa[11–14].

Identified by strong oceanic fronts, western boundary currents also typically act as barriers to cross-stream exchange. But eddies can drive cross-stream fluxes that deform the front and impact adjacent coastal seas; seas that feed and support both marine and human communities[7]. In the Agulhas Current, for example, meanders—mesoscale $\mathcal{O}$(100 km) excursions of the current—and frontal eddies—submesoscale $\mathcal{O}$(10 km) disturbances that grow along the current's sharp inshore front—can dramatically warm and/or cool South African shelf seas by driving intermittent downwelling and/or upwelling over the continental slope[15–17]. Upwelling inshore of western boundary currents supplies nutrients to coastal ecosystems[18] and influences shelf-sea productivity[19], although it often goes undetected from space due to overlying warmer waters[20].

Thirty years ago, Lutjeharms et al.[21] hypothesized that climate change could exacerbate eddying in the Agulhas Current, changing ecology and rainfall along the adjacent South African coast. Since then, satellite and in situ observations of the Agulhas Current are pointing to more eddies[1] and this trend has been linked to a reduction in the meridional heat transport of the Indian Ocean and to rapid warming of the entire basin over the last decades[22]. However, the role of eddies in both the reduction in meridional heat transport associated with the Agulhas Current[22] and the rapid warming observed in the system from space[14] is yet to be understood. The net effect of more eddying on adjacent shelf seas remains unaddressed.

Here we use a continuous two-year time series of temperature, salinity and velocity observations recorded by the Agulhas System Climate Array (ASCA) at 34° S[13,23], to study eddy energetics and quantify cross-shelf eddy fluxes in the Agulhas Current. We find that eddying of the Agulhas Current cools shelf waters along the southeast coast of Africa, implying an increase in nutrient supply to South African coastal waters with climate change. Most of this offshore eddy heat flux is driven

[1]School of Ocean and Earth Science, University of Southampton, Southampton, UK. [2]Rosenstiel School of Marine, Atmospheric and Earth Science, University of Miami, Miami, FL, USA. e-mail: k.gunn@soton.ac.uk; lbeal@miami.edu

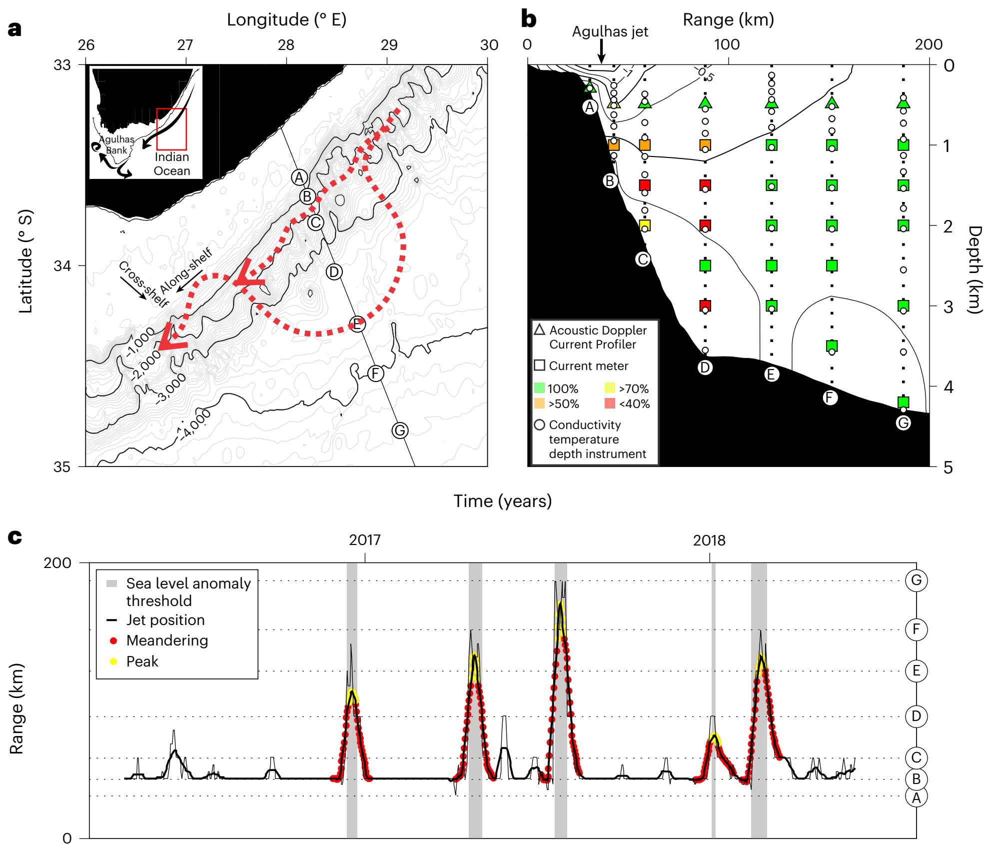

Fig. 1 | Seven moorings capture the Agulhas Current and its meandering. **a**, Mooring array (A–G) at nominally 34° S. Grey lines represent 100-m isobaths and black lines represent 1,000-m isobaths. Red dashed arrows illustrate the current in a typical linear state and in a meandering state. Inset shows the study region (red box) within the wider Agulhas system. **b**, Vertical cross-section of the moored instrumentation (symbols) and the time-mean current structure (contours every 0.25 m s^{-1}). Colours represent percentage data recovery (refer to key). **c**, Time series of current core position at 200-m depth. Meander (red) and peak-meander (yellow) times comprise approximately 10% of the 26-month record and can be separated from times when the current is linear. Grey shading defines meanders using sea level anomaly thresholds[1].

by frequent frontal eddies at the submesoscale that interact with the sloping boundary. We also find that eddying boosts stratification in the Agulhas Current, in addition to the broadening previously reported[1], explaining how rapid surface warming[24] can co-exist with a reduction in poleward heat transport[22]. More broadly, our work, along with evidence from other studies, suggests that intensifying eddies are likely to impact all subtropical western boundary currents similarly, independent of differing regional tendencies in wind forcing and overturning[25–27].

Linear and meandering states of the Agulhas Current

Eddying in the Agulhas Current is related to different instability processes dependent on whether the current is attached to the slope or separated from the slope during a meander. Therefore, we first separate our two-year time series of the current into linear and meandering states (Fig. 1 and Extended Data Figs. 1 and 2).

In the linear state, almost 90% of the time, the southwestward-flowing Agulhas Current is attached to the South African continental slope[12,23] (Extended Data Fig. 2a–d). The core of the current, with maximum velocities, is sited just offshore of the shelf-break in 1,000 m of water, at mooring B of our array. Mooring A is consistently located inshore of the current core and the mean flow between A and B has a clockwise velocity gradient, or cyclonic shear. Elsewhere across the array, offshore of the current core and in deeper waters, the mean flow exhibits anticyclonic shear.

The Agulhas Current is found in a meandering state for 10% of the time series (Fig. 1c). During a meander, the core of the current is detached from the boundary and typically displaced more than 100 km offshore at mooring E (Extended Data Fig. 2e–h). The meandering current is slower, broader and deeper-reaching than its linear counterpart, with uplifted temperature and salinity surfaces[1,13,15,23].

Eddy characteristics

Eddies and their fluxes arise from instabilities in the Agulhas Current that transfer energy from the mean flow to eddying scales (that is, variability not captured by the mean, typically at smaller spatial scales)[28–30]. Barotropic instabilities are driven by lateral velocity gradients (shear) and involve a conversion of mean kinetic energy to eddy kinetic energy (equation (1) and Extended Data Fig. 3). Baroclinic instabilities are driven by lateral density gradients and involve the conversion of potential energy to eddy potential energy (equation (2)). We are unable to close the full Lorenz energy cycle using our two-dimensional mooring dataset, which includes the conversion between eddy potential and eddy kinetic energy (Methods).

Submesoscale frontal eddying during linear state

We find that in a linear state the cyclonic side of the Agulhas Current is subject to baroclinic instability. There are ~40 submesoscale, $\mathcal{O}$(10 km), events when potential energy is converted to eddy potential energy (red shading between moorings A and B in Fig. 2b). These submesoscale frontal eddies resemble those in classic two-layer simulations[31], as well as those observed in other western boundary currents[32,33]. Farther south in the Agulhas Current, frontal eddies have been related to barotropic instability[34,35]. Here the linear cyclonic flow

https://doi.org/10.1038/s41558-026-02599-9

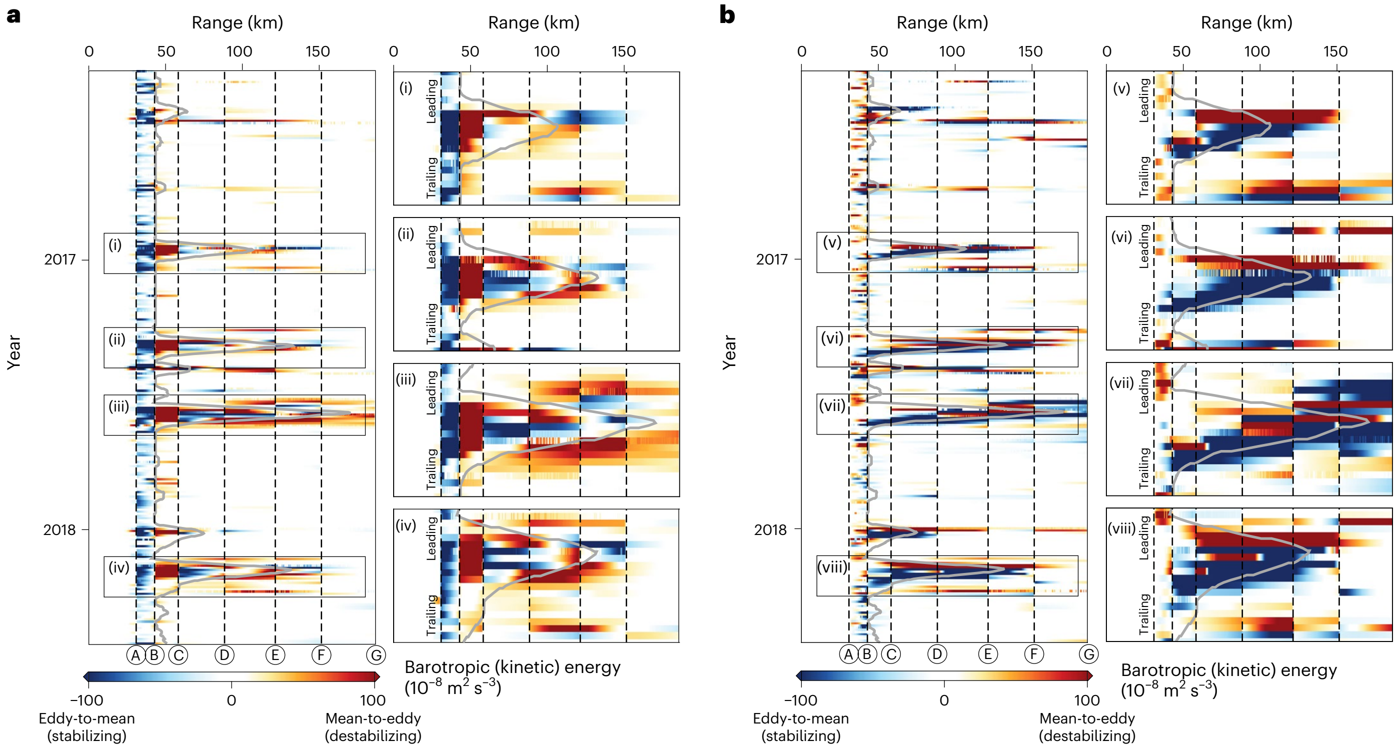

Fig. 2 | Barotropic (kinetic) and baroclinic (potential) energy conversions play competing roles in the stability of the Agulhas Current jet. a,b, Hovmöller diagrams showing the 100–1,000 m depth-averaged barotropic (**a**) and baroclinic (**b**) energy conversions across the array. Red shading indicates a destabilizing energy transfer from the mean flow to eddies, while blue indicates a stabilizing transfer from eddies to the mean flow. The grey line tracks the current core position. Detailed views of barotropic (i–iv) and baroclinic (v–viii) conversions centred on four meanders.

Table 1 | Mean-to-eddy energy transfer in the Agulhas Current

Relative location	Mooring	26-month time series		Linear current		Meandering current	
		BT	BC	BT	BC	BT	BC
Inshore (cyclonic)	A	−125	4	−114	4	−83	6
Current core	B	6	−5	−1	0	5	−5
Offshore (anticyclonic)	C	1	−10	2	−2	−2	−11
Offshore	D	10	−12	4	−2	18	−13
Offshore	E	5	−10	2	−2	6	−2
Offshore	F	2	−3	0	0	4	−5
Positive		Mean-to-eddy (destabilizing)					
Negative		Eddy-to-mean (stabilizing)					

Time-mean energy conversions are averaged over 100–1,000 m at each mooring for the full 26-month time series; 'linear' when the current is over the slope; 'meandering' when the current is detached from the slope. Values are $\times 10^{-8}$ m^2 s^{-3} and have an error of $\pm 2\times 10^{-8}$ m^2 s^{-3}. BT, barotropic (kinetic energy conversion; equation (1)); BC, baroclinic (potential energy conversion; equation (2)).

has barotropic stability: on average, barotropic (kinetic) energy transfer is negative, from the eddies back to the mean flow (blue shading between moorings A and B in Fig. 2a).

The cumulative effect of all ~40 frontal eddies can be diagnosed from our continuous observations. Baroclinic conversion slowly drains potential energy from the cyclonic mean flow over time at a rate of $(4 \pm 2) \times 10^{-8}$ m^2 s^{-3} (mooring A in Table 1 and Extended Data Fig. 4d,f). Conversely, barotropic conversion strongly reinforces the flow at a rate of $(-114 \pm 2) \times 10^{-8}$ m^2 s^{-3} through conversion of eddy kinetic energy to mean kinetic energy (Extended Data Fig. 4c,e). Hence, frontal eddies tend to slump density surfaces across the inshore edge of the Agulhas Current, while simultaneously strengthening the depth-mean flow over time. Enhanced bottom velocities are implied. These changes to the current can be interpreted as an onshore shift of the inshore front, as noted for the Gulf Stream and in high-resolution climate models[27,36].

Meandering state

During a meandering state, energy transfer from barotropic and baroclinic instabilities of the current are out of phase. Solitary mesoscale meanders propagate from upstream[37,38], changing the current's curvature and making the flow barotropically unstable. Mean-to-eddy kinetic energy conversion occurs in bursts at the leading and trailing edges of the meander, separated by opposing eddy-to-mean conversion in the meander trough (Fig. 2a(i)–(iv)). These bursts of energy loss from the mean flow arise from convergence and then divergence as the current negotiates the meander[39]. Deceleration of the fast-moving current into the trailing edge of the meander causes convergence, downwelling and

https://doi.org/10.1038/s41558-026-02599-9

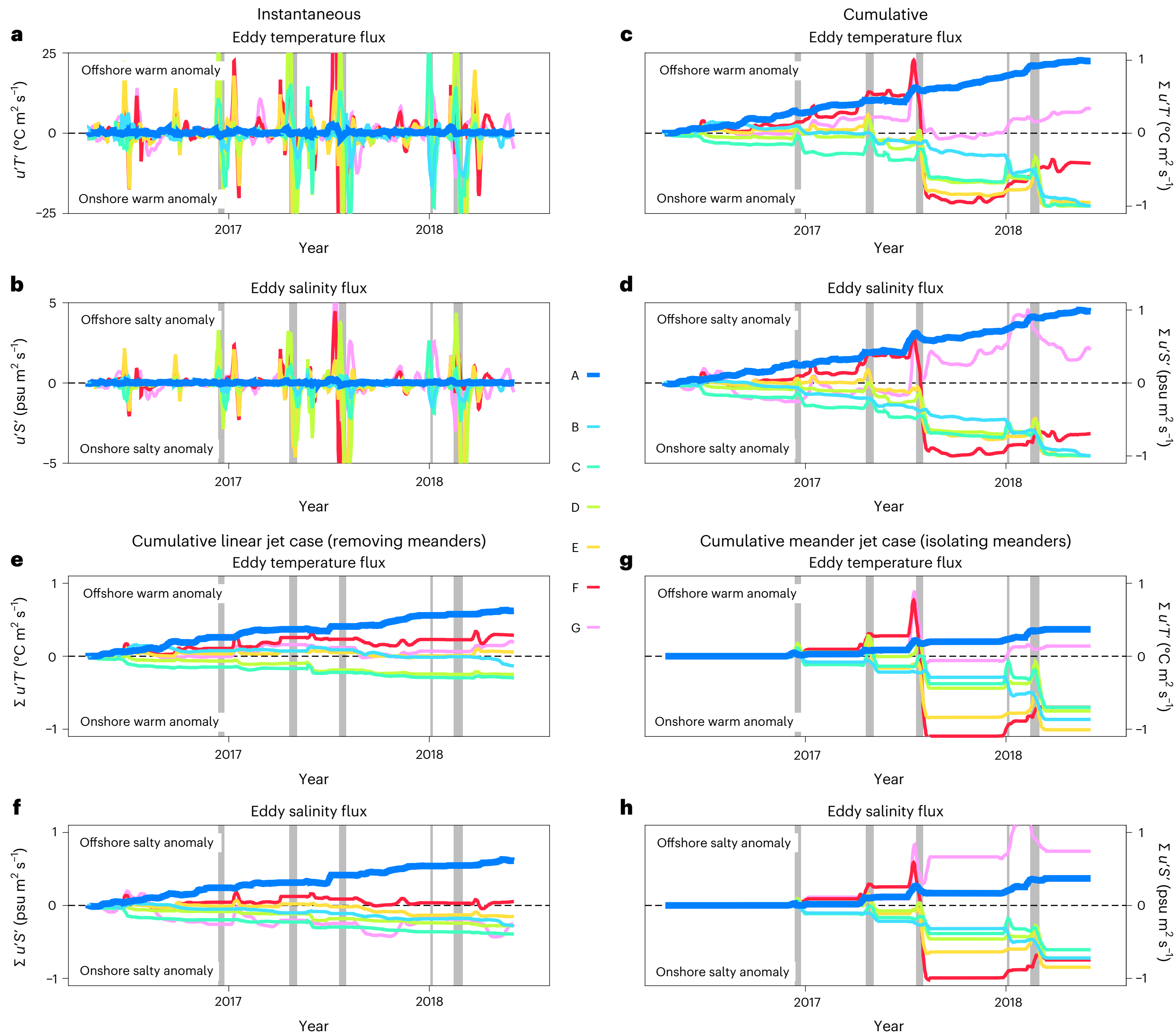

Fig. 3 | Eddy fluxes are alternating, but accumulate into robust tendencies either side of the current core. a,**b**, Instantaneous eddy temperature (**a**) and salinity (**b**) fluxes averaged over 100–1,000 m at each mooring (see key). Positive fluxes indicate offshore movement of heat and salt. Thick blue line depicts eddy fluxes inshore of the current core (i.e., mooring A). The largest instantaneous eddy fluxes coincide with meanders (grey shading). **c**,**d**, Cumulative eddy temperature (**c**) and salinity (**d**) fluxes over the full 26-month time series. **e**,**f**, Cumulative temperature (**e**) and salinity (**f**) fluxes for linear current (removing meanders), normalized by the total cumulative eddy fluxes (**c**,**d**). **g**,**h**, Cumulative temperature (**g**) and salinity (**h**) fluxes for meandering current (isolating meanders), normalized by the total cumulative eddy fluxes (**c**,**d**).

cyclonic spin-up; acceleration out of the leading edge causes divergence, upwelling and anticyclonic spin-up.

Baroclinic energy conversion from mean-to-eddy occurs as the meander grows, followed by eddy-to-mean as it passes (Fig. 2b(v)–(viii)). Potential energy is drained from the mean flow at first, until the meander trough, and then fed back into the current. Similar processes have been observed in other boundary currents, but mostly after detachment from the western boundary[39,40].

Over time, the net effect of mesoscale meanders on the Agulhas Current is to feed potential energy and drain kinetic energy on its anticyclonic side, while feeding kinetic energy and draining potential energy on its cyclonic side (Table 1 and Extended Data Fig. 4h). Hence, meandering uplifts density surfaces and weakens the depth-mean flow on the offshore side of the current, while on the onshore side, meandering slumps density surfaces and strengthens the depth-mean flow (Fig. 4). Meanders have the same tendency as frontal eddies on the inshore side of the current.

In summary, eddies—meanders and frontal instabilities together—have contrasting impacts on the cyclonic versus the anticyclonic side of the Agulhas Current. Eddies create a mixing regime onshore of the current core, where stratification is reduced and the depth-mean current is strengthened, but they create a stirring regime offshore of the current core, where stratification is enhanced and the current broadens.

Eddy fluxes

Next we quantify the cross-shelf eddy fluxes of heat and salt that are driven by the stirring and mixing regimes we found (Fig. 3). Eddy fluxes result from covariances of fluctuating cross-shelf velocity with

 https://doi.org/10.1038/s41558-026-02599-9

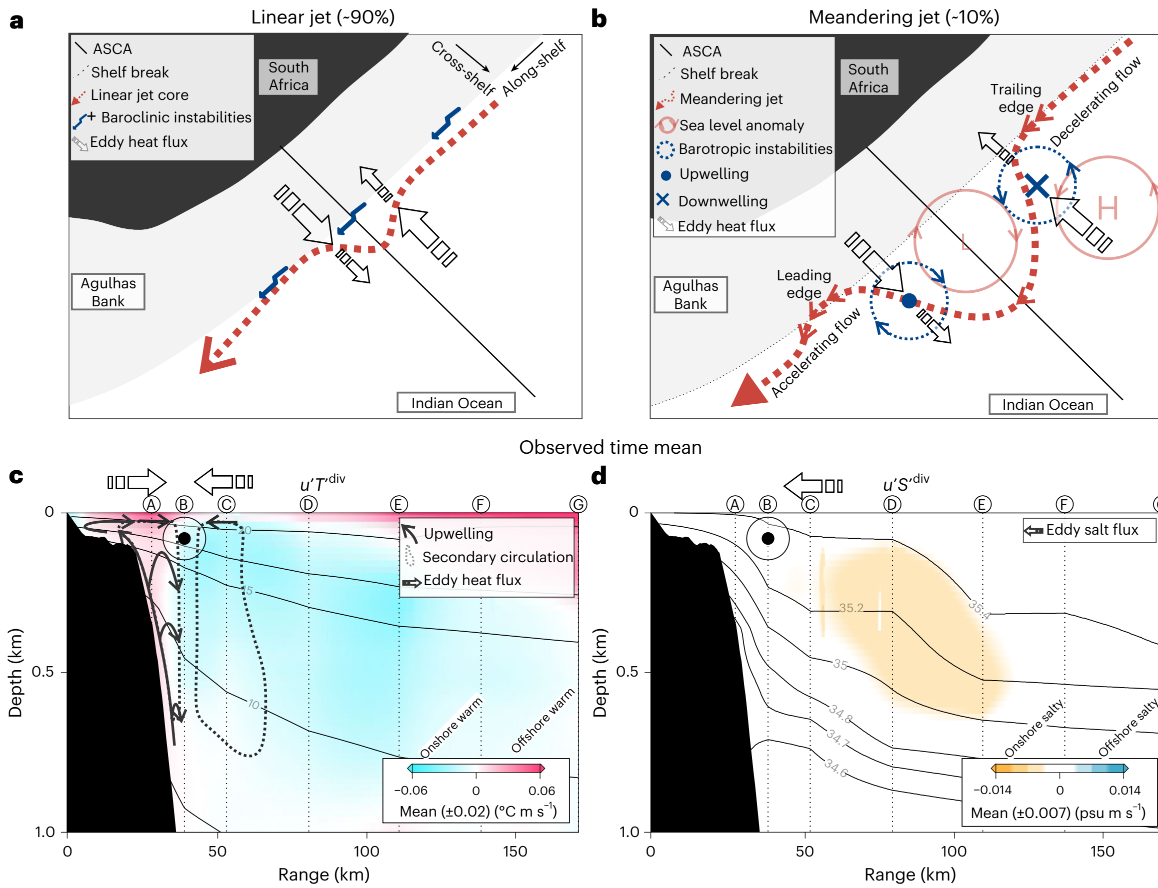

Fig. 4 | Opposing eddy fluxes at the leading and trailing edges of frontal eddies and meanders accumulate to drive a net flux of heat and salt towards the current core, revealing an eddy-driven secondary circulation. **a**, In the linear state, submesoscale frontal eddies cause alternating cross-shore eddy fluxes that accumulate to drain baroclinic energy from the mean cyclonic flow while feeding barotropic energy into it. The result is an intensification of the current over the slope. **b**, In the meandering state, the jet decelerates as it enters the trailing edge of the meander and accelerates as it leaves the leading edge, causing convergence then divergence, which drives opposing cross-shore eddy fluxes. The net effect of meanders is to drain barotropic energy from the mean anticyclonic flow while feeding baroclinic energy into it, lifting and broadening the current offshore. The net effect on the cyclonic side is the same as that of the frontal eddies. H, high; L, low. **c**,**d**, In the cross-section, the time-mean eddy temperature ($u'T'$) flux (**c**) and the time-mean eddy salinity ($u'S'$) flux (**d**) act to move heat and salt towards the core of the current. This is achieved by the presence of an eddy-driven secondary, or overturning, circulation with upwelling of cool waters onto the shelf and downwelling at the current core.

fluctuating temperature and salinity. We consider only the divergent eddy fluxes—those that represent true irreversible mixing across property gradients—by separating the non-divergent, rotational eddy fluxes[41,42]. Positive fluxes correspond to heat and salt moving offshore (Methods and Extended Data Fig. 5).

As expected, we find that both $\mathcal{O}$(10 km)-scale frontal eddies and $\mathcal{O}$(100 km)-scale meanders are associated with positive eddy fluxes as the Agulhas Current is displaced offshore followed by negative eddy fluxes as the current returns onshore (Fig. 3a–g). These instantaneous fluxes largely cancel each other out and the net or cumulative eddy fluxes are an order of magnitude smaller. At the far-offshore moorings (F and G), the eddy flux tendencies are dominated by a single extreme meander and are not robust. Everywhere else, we find robust tendencies in the net eddy fluxes, and a pattern emerges that is consistent with known dynamics.

On average, eddies transport heat and salt towards the current core (Fig. 3e–h). That is, heat and salt move away from the shelf on the inshore cyclonic side of the current (mooring A) and towards the shelf across the offshore anticyclonic side (moorings B–E). The net result is a cooling of adjacent South African shelf waters, while the core of the current becomes warmer and saltier (Fig. 4).

Frontal eddies dominate the cooling of shelf waters over time, even while individual meanders cause much larger eddy fluxes. Frontal eddies occur ten times more often than meanders, and are responsible for two thirds of the cumulative eddy heat flux on the inshore side of the current (compare dark blue lines in Fig. 3c,d with those in Fig. 3e,f). Meanders drive most of the eddy fluxes farther offshore, on the anticyclonic side of the current (compare red and pink lines in Fig. 3c,d with those in Fig. 3g,h).

The pattern of eddy flux tendencies that we find in the Agulhas Current are consistent with an eddy-driven secondary, or overturning, circulation (Fig. 4c). This secondary circulation can be predicted using turbulence closure theory, which relates unresolved turbulent motions at the sloping boundary to upwelling or downwelling, dependent on the vorticity of the flow, the bottom slope and bottom stress[25]. For a western boundary current that has mean cyclonic shear at the boundary, 'topostrophy' is negative and the work of eddies on the sloping topography will tend to pump cool, deep waters upward and onshore[25,43], resulting in the offshore eddy heat flux that we observe between moorings A and B (Fig. 3e). Net upwelling is balanced by mixing and downwelling farther offshore, signified by the convergent eddy fluxes we find in the core of the current (Fig. 4c). The upwelling tendency arises from the cumulative effect of all eddies over time, no matter the sense of rotation of each individual eddy, as long as the eddies are embedded in a mean flow that has negative topostrophy. The theory does not apply to a single eddy event, which may cause net upwelling or downwelling.

Western boundary upwelling can also be understood as 'Ekman veering' by parameterizing unresolved turbulence as an eddy viscosity[44]. The frictional bottom boundary veers the overlying current to the right in the southern hemisphere, inducing onshore transport and associated upwelling. Such upwelling of cold waters inshore of western boundary currents has been observed, for example, in the East Australia Current[45], but is typically hidden from satellite observations by overlying warm waters[20].

The dynamics implied by these net eddy fluxes are consistent with our energy analysis results above. Eddies pump cold, dense waters upward and onshore over the continental slope, with intense mixing above. This process cools adjacent South African shelf waters, slumps the inshore front and increases the depth-mean flow on the cyclonic side of the current. Meanwhile, away from the sloping boundary, eddies predominantly stir heat and salt along isopycnals (Fig. 4d). This process broadens the current and increases stratification on the anticyclonic side of the current.

Discussion

There are several limitations to our results. The net eddy fluxes we find are small, of the same order of magnitude as our estimated errors, and this introduces significant statistical uncertainty. That said, the net eddy fluxes are consistent with known dynamics and also with independent measures of change in the Agulhas Current, such as broadening and rapid surface warming.

There are missing data in the upper water column, where intense currents blow the moored instrumentation down, sometimes hundreds of metres[13,23]. We were able to mitigate the effect of blow-down for velocity by deploying current meters that use acoustics to measure the flow remotely from 500 m to 600 m below. But temperature and salinity data require local measurement. Blow-down, therefore, contributes to large uncertainty in our near-surface eddy flux estimates and remains a serious limitation to climate observations in strong ocean currents.

Finally, our measurements are limited to a single latitude in the Agulhas Current. At other latitudes or in other western boundary currents—where flow depth, bottom slope and eddy energetics differ—the sensitivity of cross-stream eddy fluxes and the resulting frontal adjustment may vary. For example, the balance between barotropic and baroclinic energy conversion depends on region[35,46,47], depth[48] and time[49], and eddies can manifest locally as whirls, waves or rectified mean flow. Regional trends in wind forcing[50,51] and overturning circulation[49,52] may also superpose further adjustments. Despite these factors, the tendency for eddies to drive upwelling inshore of subtropical western boundary currents is universal[44,53]. Consistent with this upwelling theory are lower rates of long-term subsurface warming on shelf seas inshore of the East Australia Current compared to shelf seas after the current has detached[26]. Moreover, the eddy flux tendencies that we find can explain the rapid surface warming and onshore shifting observed in all subtropical western boundary currents[11,27,36,51,54].

One potential implication of more upwelling of cold waters inshore of subtropical western boundary currents is an increase in nutrient supply and a potential boost to coastal ecosystems and regional commercial fisheries. Evidence for this is mixed. Coastal phytoplankton blooms have expanded in the twenty-first century, particularly around subtropical gyres[55]. Around South Africa, chokka squid[56] and Natal corals[57] may depend on Agulhas-driven upwelling for their spawning and survival. However, more eddying can reduce chokka squid recruitment[58,59], and an intense cold event in the Agulhas Current in 2021 was linked to the death of 81 species[19]. Factoring in the eddy-driven boost in stratification and rapid warming of surface waters that are accompanying more upwelling, it is likely that more extreme conditions will prevail over the shelf. We might anticipate the emergence of a 'Goldilocks zone' over the outer shelf where more nutrient-rich upwelled waters can enhance marine life, while the inner shelf, less affected by upwelling and more by surface warming, could become less productive.

Conclusions

In a warming world, where the ocean is eddying more, upwelling inshore of the Agulhas Current is increasing, cooling adjacent shelf seas and potentially enhancing coastal productivity over time. Eddying is also boosting the stratification of the Agulhas Current, leading to surface waters warming at 3–4 times the rate of the mean ocean, with cooler waters at depth. Eddies explain how rapid surface warming downstream in the Agulhas system, tied to increased continental rainfall in South Africa[14], can co-exist with a decrease in total heat flux to higher latitudes[22], and how these profound changes are happening while the volume transport of the Agulhas Current is holding steady[1].

Our findings in the Agulhas Current can be extended globally. Intensifying eddies provide a universal explanation for the warming and broadening, or shifting, of subtropical western boundary currents observed globally[36]. And using dynamical theory we may predict that more eddies will increase hidden upwelling inshore of all subtropical western boundary currents. This holds regardless of how the eddies manifest locally—as whirls, waves or rectified mean flow—and regardless of regional wind and overturning tendencies that may govern changes in boundary current strength.

There may need to be a shift in the metrics used to signify dynamical change in the ocean and to benchmark climate models. With the volume transports of the Agulhas Current[1] and Gulf Stream[60] holding steady and trends in the overturning circulation still under debate, long-term observations of eddy fluxes may better reveal climatic changes in the ocean.

Online content

Any methods, additional references, Nature Portfolio reporting summaries, source data, extended data, supplementary information, acknowledgements, peer review information; details of author contributions and competing interests; and statements of data and code availability are available at https://doi.org/10.1038/s41558-026-02599-9.

References

1. Beal, L. M. & Elipot, S. Broadening not strengthening of the Agulhas Current since the early 1990s. *Nature* https://doi.org/10.1038/nature19853 (2016).
2. Hu, H. et al. Deep-reaching acceleration of global mean ocean circulation over the past two decades. *Sci. Adv.* **6**, 7727 (2020).
3. Martínez-Moreno, J. et al. Global changes in oceanic mesoscale currents over the satellite altimetry record. *Nat. Clim. Change* **11**, 397–403 (2021).
4. Beech, N. et al. Long-term evolution of ocean eddy activity in a warming world. *Nat. Clim. Change* **12**, 910–917 (2022).
5. Guo, Y., Bachman, S., Bryan, F. & Bishop, S. Increasing trends in oceanic surface poleward eddy heat flux observed over the past three decades. *Geophys. Res. Lett.* https://doi.org/10.1029/2022GL099362 (2022).
6. Yang, H. Warming hotspots induced by more eddies. *Nat. Clim. Change* **12**, 889–890 (2022).
7. Savidge, W. B. et al. Western boundary current–subtropical continental shelf interactions. *Oceanography* **37**, 64–69 (2024).
8. Perez, E., Andres, M. & Gawarkiewicz, G. Is the regime shift in gulf stream warm core rings detected by satellite altimetry? An inter-comparison of eddy identification and tracking products. *J. Geophys. Res. Oceans* https://doi.org/10.1029/2023JC020761 (2024).
9. Palter, J. B. The role of the gulf stream in European climate. *Annu. Rev. Mar. Sci.* **7**, 113–137 (2015).
10. Wise, E. K. & Dannenberg, M. P. Reconstructed storm tracks reveal three centuries of changing moisture delivery to North America. *Sci. Adv.* **3**, 1602263 (2017).
11. Wu, L. et al. Enhanced warming over the global subtropical western boundary currents. *Nat. Clim. Change* **2**, 161–166 (2012).

12. Beal, L. M., Elipot, S., Houk, A. & Leber, G. M. Capturing the transport variability of a western boundary jet: results from the Agulhas Current Time-series Experiment (ACT). *J. Phys. Oceanogr.* https://doi.org/10.1175/jpo-d-14-0119.1 (2015).
13. McMonigal, K. et al. The impact of meanders, deepening and broadening, and seasonality on Agulhas Current temperature variability. *J. Phys. Oceanogr.* https://doi.org/10.1175/JPO-D-20-0018.1 (2020).
14. Rouault, M., Dieppois, B., Tim, N., Hünicke, B. & Zorita, E. in *Sustainability of Southern African Ecosystems Under Global Change: Science for Management and Policy Interventions* (eds Canadell, J. G. et al.) 149–168 (Springer, 2024).
15. Leber, G. M. & Beal, L. M. Local water mass modifications by a solitary meander in the Agulhas Current. *J. Geophys. Res. Oceans* **120**, 4501–4515 (2015).
16. Goschen, W. S., Bornman, T. G., Deyzel, S. H. P. & Schumann, E. H. Coastal upwelling on the far eastern Agulhas Bank associated with large meanders in the Agulhas Current. *Cont. Shelf Res.* **101**, 34–46 (2015).
17. Malan, N. et al. Agulhas current meanders facilitate shelf-slope exchange on the eastern Agulhas bank. *J. Geophys. Res. Oceans* **123**, 4762–4778 (2018).
18. Marshall, T. A., Beal, L., Sigman, D. M. & Fawcett, S. E. Instabilities across the Agulhas Current enhance upward nitrate supply in the southwest subtropical Indian Ocean. *AGU Adv.* https://doi.org/10.1029/2023AV000973 (2023).
19. Lubitz, N. et al. Climate change-driven cooling can kill marine megafauna at their distributional limits. *Nat. Clim. Change* **14**, 526–535 (2024).
20. Liao, F., Liang, X., Li, Y. & Spall, M. Hidden upwelling systems associated with major western boundary currents. *J. Geophys. Res. Oceans* https://doi.org/10.1029/2021JC017649 (2022).
21. Lutjeharms, J. R. E., Meyer, A. A., Ansorge, I. J., Eagle, G. A. & Orren, M. J. The nutrient characteristics of the Agulhas bank. *S. Afr. J. Mar. Sci.* **17**, 253–274 (1996).
22. McMonigal, K., Gunn, K. L., Beal, L., Elipot, S. & Willis, J. K. Reduction in meridional heat export contributes to recent Indian Ocean warming. *J. Phys. Oceanogr*. **52**, 329–334 (2022).
23. Gunn, K. L., Beal, L. M., Elipot, S., McMonigal, K. & Houk, A. Mixing of subtropical, central and intermediate waters driven by shifting and pulsing of the Agulhas Current. *J. Phys. Oceanogr.* **50**, 3545–3560 (2020).
24. Rouault, M., Penven, P. & Pohl, B. Warming in the Agulhas Current system since the 1980s. *Geophys. Res. Lett.* https://doi.org/10.1029/2009GL037987 (2009).
25. Holloway, G. Systematic forcing of large-scale geophysical flows by eddy-topography interaction. *J. Fluid Mech.* **184**, 463–476 (1987).
26. Malan, N., Roughan, M. & Kerry, C. The rate of coastal temperature rise adjacent to a warming western boundary current is nonuniform with latitude. *Geophys. Res. Lett.* https://doi.org/10.1029/2020GL090751 (2021).
27. Todd, R. E. & Ren, A. S. Warming and lateral shift of the gulf stream from in situ observations since 2001. *Nat. Clim. Change* **13**, 1348–1352 (2023).
28. Lorenz, E. N. Available potential energy and the maintenance of the general circulation. *Tellus* **7**, 157–167 (1955).
29. Margules, M. Über die energie der stürme. *Jahrb. K. K. Zent. Meteorol. Geodyn.* **40**, 1–26 (1903).
30. Lorenz, E. N. *The Nature and Theory of the General Circulation of the Atmosphere* No. 218, T.P. 115 (WMO, 1967).
31. Orlanski, I. & Cox, M. D. Baroclinic instability in ocean currents. *Geophys. Fluid Dyn.* **4**, 297–332 (1973).
32. Archer, M. R., Shay, L. K., Jaimes, B. & Martinez-Pedraja, J. in *Coastal Ocean Observing Systems* (eds Steele, J. H. et al.) 179–208 (Elsevier, 2015).
33. Ismail, M. F. A. & Ribbe, J. On the cross-shelf exchange driven by frontal eddies along a western boundary current during austral winter 2007. *Estuar. Coast. Shelf Sci.* **227**, 106314 (2019).
34. Krug, M., Swart, S. & Gula, J. Submesoscale cyclones in the Agulhas Current. *Geophys. Res. Lett.* **44**, 346–354 (2017).
35. Tedesco, P., Gula, J., Ménesguen, C., Penven, P. & Krug, M. Generation of submesoscale frontal eddies in the Agulhas Current. *J. Geophys. Res. Oceans* **124**, 7606–7625 (2019).
36. Yang, H. et al. Onshore intensification of subtropical western boundary currents in a warming climate. *Nat. Clim. Change* **15**, 301–307 (2025).
37. Krug, M. & Penven, P. New perspectives on natal pulses from satellite observations. *J. Geophys. Res. Oceans* **116**, 07002 (2011).
38. Elipot, S. & Beal, L. M. Characteristics, energetics, and origins of Agulhas Current meanders and their limited influence on ring shedding. *J. Phys. Oceanogr.* https://doi.org/10.1175/jpo-d-14-0254.1 (2015).
39. Lindstrom, S. S., Qian, X. & Watts, D. R. Vertical motion in the gulf stream and its relation to meanders. *J. Geophys. Res. Oceans* **102**, 8485–8503 (1997).
40. Donohue, K. A., Watts, D. R., Hamilton, P., Leben, R. & Kennelly, M. Loop current eddy formation and baroclinic instability. *Dynam. Atmos. Oceans* **76**, 195–216 (2016).
41. Marshall, J. & Shutts, G. A note on rotational and divergent eddy fluxes. *J. Phys. Oceanogr.* **11**, 1677–1680 (1981).
42. Bishop, S. P., Watts, D. R. & Donohue, K. A. Divergent eddy heat fluxes in the Kuroshio Extension at 1448°–1488°E. Part I: mean structure. *J. Phys. Oceanogr.* **43**, 1533–1550 (2013).
43. Schubert, R. et al. The ocean flows downhill near the seafloor and recirculates upward above. *Nat. Commun.* **16**, 5873 (2025).
44. Kundu, P. K. Ekman veering observed near the ocean bottom. *J. Phys. Oceanogr.* **6**, 238–242 (1976).
45. Schaeffer, A., Roughan, M. & Wood, J. E. Observed bottom boundary layer transport and uplift on the continental shelf adjacent to a western boundary current. *J. Geophys. Res. Oceans* **119**, 4922–4939 (2014).
46. Magalhães, F. C., Azevedo, J. L. L. & Oliveira, L. R. Energetics of eddy-mean flow interactions in the brazil current between 20°s and 36°s. *J. Geophys. Res. Oceans* **122**, 6129–6146 (2017).
47. Yang, Y. & Liang, X. S. On the seasonal eddy variability in the Kuroshio extension. *J. Phys. Oceanogr.* **48**, 1675–1689 (2018).
48. Cronin, M. & Watts, D. R. Eddy-mean flow interaction in the gulf stream at 68°w. Part I: eddy energetics. *J. Phys. Oceanogr.* **26**, 2107–2131 (1996).
49. Li, Q. et al. Abyssal ocean overturning slowdown and warming driven by Antarctic meltwater. *Nature* **615**, 841–847 (2023).
50. Marshall, J. & Speer, K. Closure of the meridional overturning circulation through Southern Ocean upwelling. *Nat. Geosci.* **5**, 171–180 (2012).
51. Li, J., Roughan, M. & Kerry, C. Drivers of ocean warming in the western boundary currents of the southern hemisphere. *Nat. Clim. Change* **12**, 901–909 (2022).
52. Weijer, W., Cheng, W., Garuba, O. A., Hu, A. & Nadiga, B. T. CMIP6 models predict significant 21st century decline of the Atlantic meridional overturning circulation. *Geophys. Res. Lett.* https://doi.org/10.1029/2019GL086075 (2020).
53. Holloway, G. Observing global ocean topostrophy. *J. Geophys. Res. Oceans* **113**, 07054 (2008).
54. Wang, G., Xie, S. P., Huang, R. X. & Chen, C. Robust warming pattern of global subtropical oceans and its mechanism. *J. Clim.* **28**, 8574–8584 (2015).
55. Dai, Y. et al. Coastal phytoplankton blooms expand and intensify in the 21st century. *Nature* **615**, 280–284 (2023).

https://doi.org/10.1038/s41558-026-02599-9

56. Downey, N. J., Roberts, M. J. & Baird, D. An investigation of the spawning behaviour of the chokka squid *Loligo reynaudii* and the potential effects of temperature using acoustic telemetry. *ICES J. Mar. Sci.* **67**, 231–243 (2009).
57. Wells, C., Pringle, J. & Stretch, D. D. Upwelling along the southeast African coastline and links to cold water temperature anomalies at Sodwana Bay, South Africa. *Cont. Shelf Res.* **276**, 105227 (2024).
58. Jackson, J. M., Rainville, L., Roberts, M. J., McQuaid, C. D. & Lutjeharms, J. R. E. Mesoscale bio-physical interactions between the Agulhas Current and the Agulhas Bank, South Africa. *Cont. Shelf Res.* **49**, 10–24 (2012).
59. Jebri, F. et al. Unravelling links between squid catch variations and biophysical mechanisms in South African waters. *Deep-Sea Res. II: Top. Stud. Oceanogr.* **196**, 105028 (2022).
60. Volkov, D. L. et al. Florida current transport observations reveal four decades of steady state. *Nat. Commun.* **15**, 7780 (2024).

Publisher's note Springer Nature remains neutral with regard to jurisdictional claims in published maps and institutional affiliations.

Methods

We used two years of continuous temperature, salinity and velocity measurements from a mooring array across the Agulhas Current at 34° S[13,23]. The vertical resolution of velocity data from Acoustic Doppler Current Profilers in the upper water column is 16 m, while all other data are presented as point measurements, as depicted in Fig. 1a,b. The array was co-located with a satellite altimetry ground track providing sea level anomalies at 8-km resolution[12]. The mooring data were carefully extrapolated to the surface using satellite measurements, interpolated onto a 500 m × 20 dbar spatial grid and filtered to 20-hour intervals, removing tides and inertial cycles[13,23]. For our study of cross-shelf eddy fluxes, we rotated Cartesian velocities by +14° onto along-shelf and cross-shelf components, where along-shelf is parallel to the Agulhas Current's mean flow (Extended Data Fig. 1). Using time-dependent streamwise coordinates did not change our results.

Linear and meandering flow

We determined the displacement of the current core (its distance from the coast) at each time step using the maximum southwestward flow at a depth of 200 m. Five mesoscale meander events are identified when the sea level anomaly at mooring C drops below −0.2 m, consistent with refs. 1,38. Using the maximum displacement of the jet, we then defined individual meander events as 20-day periods centred on the five largest displacement peaks. This classification allowed us to separate the flow into two states: linear flow, which includes ~10-km-scale frontal eddies, and meandering flow, which isolates the ~100-km-scale offshore excursions of the jet. We further defined the meander 'trough' as the ±3-day period around the maximum displacement, and the 'leading' and 'trailing' edges as the 10 days immediately preceding and following the trough (Fig. 1c and Extended Data Fig. 2).

Instabilities

Barotropic and baroclinic instabilities mediate the exchange of kinetic and potential energy between the mean flow and the eddies[28]. Therefore, we can identify these instabilities by estimating energy conversion rates for kinetic (barotropic) and potential (baroclinic) energy (in $m^2 s^{-3}$).

Barotropic (BT) energy conversion is calculated as[38]

$$\mathrm{BT} = -u'u'\frac{\mathrm{d}\bar{u}}{\mathrm{d}x} - u'v'\frac{\mathrm{d}\bar{v}}{\mathrm{d}x} + v'v'\frac{\mathrm{d}\bar{u}}{\mathrm{d}x}, \qquad (1)$$

where u' and v' are velocity fluctuations from the time-mean cross-shelf (u) and along-shelf (v) flows, respectively, and $\frac{\mathrm{d}\bar{u}}{\mathrm{d}x}$ and $\frac{\mathrm{d}\bar{v}}{\mathrm{d}x}$ are the spatially varying horizontal (x) gradients of the time-mean cross-shelf and along-shelf velocities.

Baroclinic (BC) energy conversion is calculated as[61]

$$\mathrm{BC} = -\frac{g\alpha}{\frac{\mathrm{d}\bar{T}}{\mathrm{d}z}}\left(u'T'\frac{\mathrm{d}\bar{T}}{\mathrm{d}x}\right), \qquad (2)$$

where g is gravitational acceleration, α is the thermal expansion coefficient and $u'T'$ is the covariance of cross-shelf velocity and temperature fluctuations; $\frac{\mathrm{d}\bar{T}}{\mathrm{d}z}$ and $\frac{\mathrm{d}\bar{T}}{\mathrm{d}x}$ are the spatially varying vertical (z) and horizontal (x) gradients of the time-mean conservative temperature field. For both BT and BC, positive values signify growing instabilities with energy transfer from the mean flow to the eddies (jet destabilizing).

The mooring configuration imposes several limitations on the quantification of energy conversion terms. First, in estimating barotropic conversion, we assume horizontal non-divergence to replace the unmeasured $\partial\bar{v}/\partial y$ with $-\partial\bar{u}/\partial x$. An alternative barotropic formulation that neglects both $\partial\bar{u}/\partial y$ and $\partial\bar{v}/\partial y$ yields close agreement with our primary estimate ($r^2 = 0.94$; Extended Data Fig. 3), indicating that this assumption does not strongly affect our results (Fig. 2 and Extended Data Fig. 4). Second, lacking accurate measurements of vertical velocity fluctuations (w'), we are unable to calculate the conversion of eddy potential energy to eddy kinetic energy and close the full eddy energy cycle. Nevertheless, this conversion is thought to be highly efficient in western boundary currents[48,62], suggesting that the inferred energy pathways between potential and kinetic energy are likely. Third, the two-dimensional mooring array does not provide along-shelf components of energy conversion, but these terms are typically much smaller than the cross-shelf components[63]. Energy analyses using high-resolution models show that cross-frontal terms alone provide a good approximation of the total energy conversion[35]. Finally, we use temperature alone to characterize baroclinic processes, assuming that salinity makes a comparatively small contribution to density variability in this region.

Divergent eddy fluxes

The term 'eddy' denotes any fluctuation from the time-mean flow, with no particular dynamics implied. The total eddy covariance terms for each variable (u'^{total}, v'^{total}, T'^{total} and S'^{total}) were calculated as deviations of the instantaneous measurement (u) from the time mean ($\bar{u}$): $u'^{\mathrm{total}} = u - \bar{u}$. For the eddy covariance terms of the linear and meandering states, $\bar{u}$ is calculated separately as the time mean of each state. We calculated total cross-shelf eddy heat and salt fluxes from the covariances of fluctuating conservative temperature and absolute salinity with cross-shelf velocity: $u'T'^{\mathrm{total}}$ (°C m s^{-1}) and $u'S'^{\mathrm{total}}$ (psu m s^{-1}).

Only eddy fluxes that represent the displacement of water parcels across temperature or salinity gradients cause irreversible change. Hence, we decompose the total eddy heat and salt fluxes into divergent—resulting in a net change of properties—and non-divergent—purely rotational—components. Assuming property gradients are large compared to the scale of the eddies, and assuming rotational water parcels conserve enstrophy[41,48], we calculate the time-mean non-divergent eddy flux as

$$\overline{u'T'}^{\mathrm{nondiv}} = \frac{1}{2}\frac{\mathrm{d}\psi}{\mathrm{d}T}\frac{\mathrm{d}\overline{T'^2}}{\mathrm{d}x}, \qquad (3)$$

where ψ is the stream function of the flow, and $\frac{\mathrm{d}\overline{T'^2}}{\mathrm{d}x}$ is the horizontal gradient of the squared temperature variance (equivalent to equation (8) of ref. 48).

The assumptions for this decomposition are reasonable when the stream function of the flow is near parallel with the isotherms, such that rotational flow follows temperature surfaces and the scaling factor $\frac{\mathrm{d}\psi}{\mathrm{d}T}$ is more or less constant over time[41,42,48]. We test this by calculating the stream function $\psi = \int v\mathrm{d}x$ directly from our mooring data, and comparing the change in stream function along a surface of constant depth with the change in temperature (Extended Data Fig. 5). There is a linear fit between these over a depth interval of 100–1,000 m, where $r^2 > 0.9$. Near the surface, the fit degrades due to the influence of the Ekman layer, while at depth the fit degrades due to the increasing influence of the barotropic flow. Thus, we constrain our eddy flux analysis to between 100 m and 1,000 m of the water column; $\frac{\mathrm{d}\psi}{\mathrm{d}T}$ is estimated at each mooring every 20 m depth and smoothed using a centred moving average over a 400-m vertical window.

Finally, we obtain the divergent eddy fluxes by removing the estimated non-divergent fluxes of equation (3) from the total fluxes

$$u'T' = u'T'^{\mathrm{total}} - \overline{u'T'}^{\mathrm{nondiv}}. \qquad (4)$$

The resulting divergent eddy fluxes are very similar to those estimated using an alternative and independent method[42], wherein they are approximated from the cross-shelf barotropic (bottom) flow. We report instantaneous eddy fluxes at each mooring as the depth integral from 100 m to 1,000 m, and we estimate the eddy flux tendencies by cumulatively summing the depth-integrated eddy fluxes over time (Fig. 3).

Positive $u'T'$ and $u'S'$ indicate onshore fluxes of cold and fresh water or, equivalently, offshore fluxes of warm and salty water. Negative values indicate anomalous onshore flux of heat and salt.

Uncertainties

To evaluate uncertainties in the energy conversion terms and eddy fluxes, we propagate the mooring measurement errors reported by refs. 13,23, which include sampling, instrumental and interpolation errors (Fig. 1b). For temperature, salinity and velocity, these are $\sigma_T = 0.14$ °C, $\sigma_S = 0.05$ psu and $\sigma_u = 0.01$ m s^{-1}, respectively. Errors in perturbation quantities are larger by a factor of approximately $\sqrt{2}$ (ref. 64). Using independent error-propagation rules (for example, relative errors add when quantities are multiplied), we estimate uncertainties on the order of 2×10^{-8} m^2 s^{-3} for the barotropic and baroclinic energy conversion terms. For the barotropic energy conversion we only propagate the errors for the second term, as it is about twice as large as the others. Using inferred vertical velocities[18], we find that the uncertainty associated with horizontal divergence is small (~5%) relative to the propagated measurement errors. The errors of the cross-shelf eddy fluxes are $\sigma_{u'T'} \approx 0.02$ °C m s^{-1} and $\sigma_{u'S'} \approx 0.007$ psu m s^{-1}.

Data availability

Analysis was completed using The MathWorks Inc. (2022) MATLAB v.24.2.0.2773142 (R2024b)[65]. Figures were made with GMT5[66]. Temperature, salinity and velocity recorded by the ASCA and Agulhas Current Time-series experiments can be obtained from https://beal-agulhas.earth.miami.edu/data-and-products/index.html.

Code availability

The analysis code is available via Zenodo at https://doi.org/10.5281/zenodo.17084587 (ref. 67).

References

61. Phillips, H. E. & Rintoul, S. R. Eddy variability and energetics from direct current measurements in the Antarctic circumpolar current south of Australia. *J. Phys. Oceanogr.* **30**, 3050–3076 (2000).
62. He, Y., Zhou, M. & Kang, D. Strong eddy kinetic energy anomalies induced by baroclinic instability in the southwest region of the Kerguelen Plateau, East Antarctica. *J. Geophys. Res. Oceans* https://doi.org/10.1029/2023JC020667 (2024).
63. Beal, L. M., Chereskin, T. K., Lenn, Y. D. & Elipot, S. The sources and mixing characteristics of the Agulhas Current. *J. Phys. Oceanogr.* **36**, 2060–2074 (2006).
64. Burroughs, C. B., Fischer, R. W. & Kern, F. R. An introduction to statistical energy analysis. *J. Acoust. Soc. Am.* **101**, 1779–1789 (1997).
65. Statistics and Machine Learning Toolbox https://www.mathworks.com/help/stats/index.html (2024).
66. Wessel, P., Smith, W. H. F., Scharroo, R., Luis, J. & Wobbe, F. Generic Mapping Tools: improved version released. https://doi.org/10.1002/2013EO450001 (2013).
67. Gunn, K. Energy conversion and eddy flux code. *Zenodo* https://doi.org/10.5281/zenodo.17084587 (2026).

Acknowledgements

Collection of the ASCA data was made possible through collaboration with J. Hermes and the South African Environmental Observation Network Egagasini Node, with local ship time supported by the National Research Foundation of South Africa. We thank the mooring technicians of NautiBuoys, Cape Town, for the fabrication and deployment of the moorings. We gratefully acknowledge K. McMonigal, S. Elipot, A. Houk, M. Graham and all those aboard the ASCA cruises, whose efforts laid the foundation for this work. L.M.B. acknowledges support from US National Science Foundation Awards 1459543 and 2148676.

Author contributions

K.L.G.: methodology, visualization, software, validation, analysis, writing—original draft. L.M.B.: conceptualization, investigation, resources, project administration, funding acquisition and writing—review and editing.

Competing interests

The authors declare no competing interests.

Additional information

Extended data is available for this paper at https://doi.org/10.1038/s41558-026-02599-9.

Correspondence and requests for materials should be addressed to K. L. Gunn or L. M. Beal.

Peer review information *Nature Climate Change* thanks Neil Malan and Pauline Tedesco for their contribution to the peer review of this work.

https://doi.org/10.1038/s41558-026-02599-9

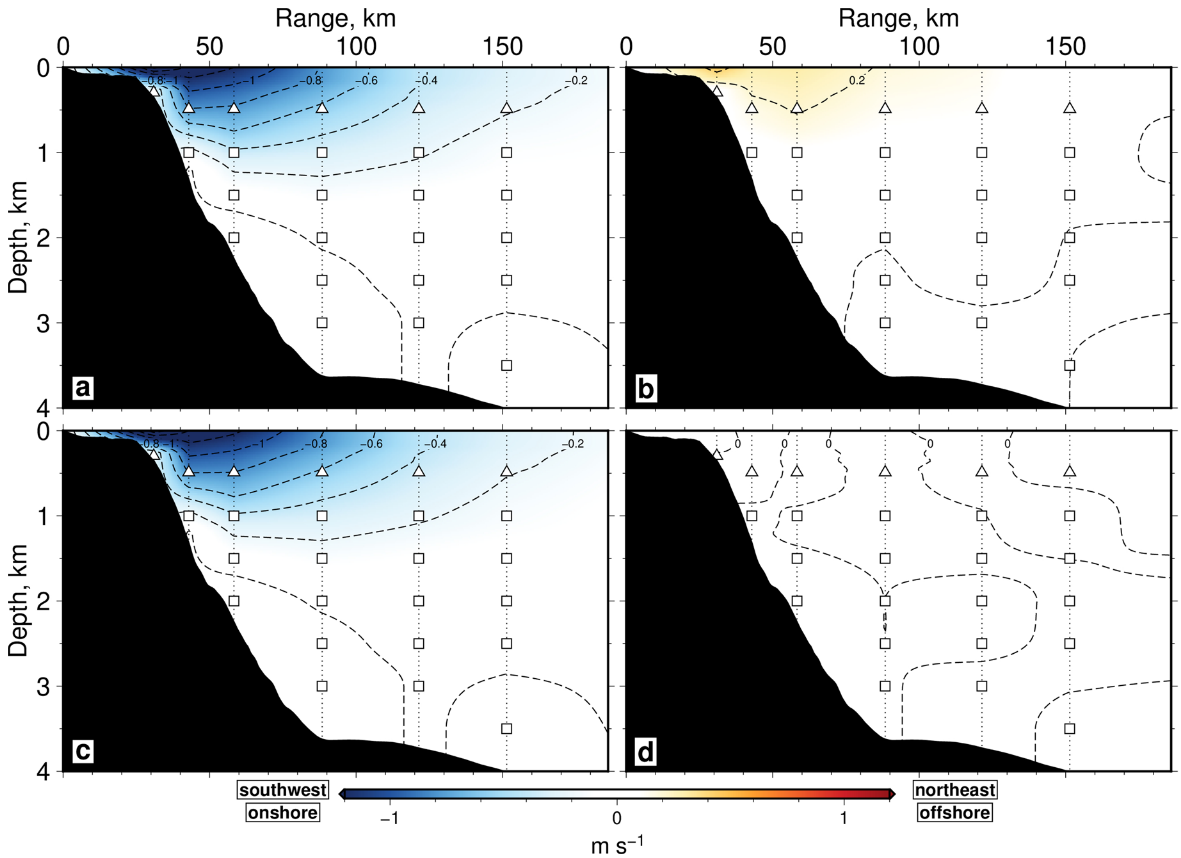

Extended Data Fig. 1 | Placing the recorded velocity field into along- and cross-shelf context using a geographic coordinate frame. (**a**,**b**) In the original instrument coordinates, the time-mean velocity is separated into cross-track (**a**) and along-track (**b**) components. (**c**,**d**) After rotation by a constant angle of 14°, the velocity field is decomposed into the dominant along-shelf flow of the Agulhas Jet (**c**) and the weaker cross-shore flow (**d**).

https://doi.org/10.1038/s41558-026-02599-9

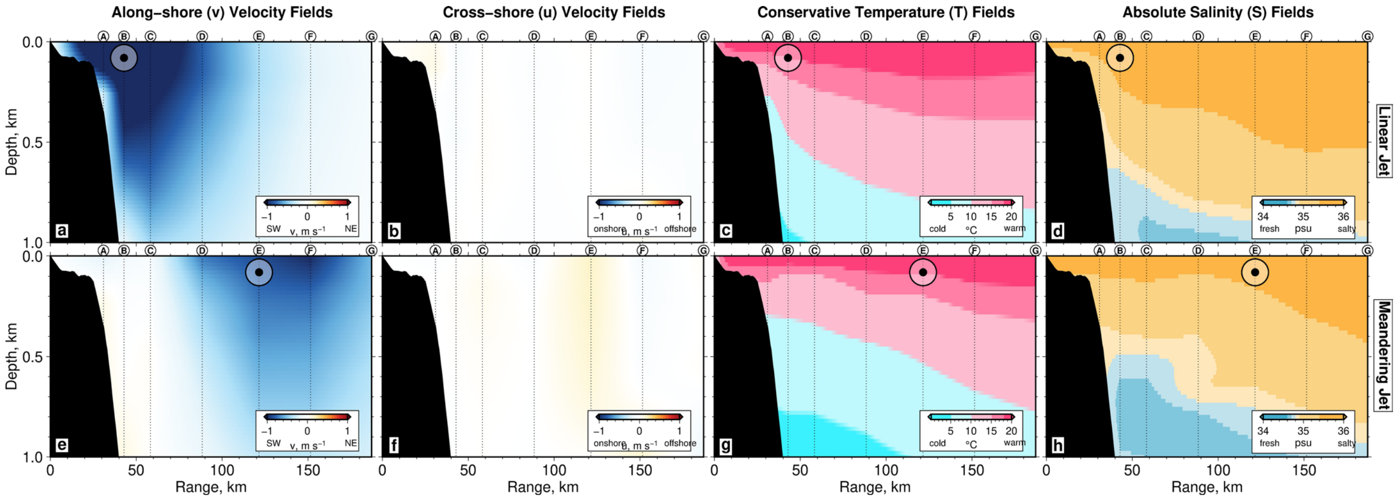

Extended Data Fig. 2 | The Agulhas Current has two distinct states: a stable linear flow (~ 90% of the time) and a meandering state that triggers reorganization of its structure. (**a**-**h**) Composite cross-sections comparing the current's structure during its linear (top row, **a**-**d**) and meandering (bottom row, **e**-**h**) states. Panels show along-shelf velocity (v), cross-shelf velocity (u), Conservative Temperature (T), and Absolute Salinity (S).

https://doi.org/10.1038/s41558-026-02599-9

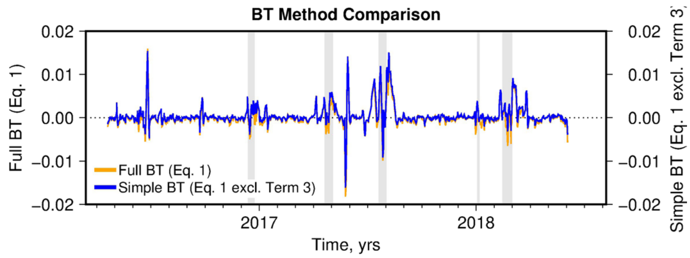

Extended Data Fig. 3 | Comparison of barotropic energy conversion estimates. Time series of full barotropic energy conversion (orange; BT estimated by Eq. 1) and a simplified formulation that omits third term removing the necessary assumption of horizontal non-divergence (blue: BT estimated by Eq. 1 excluding v'^2 du/dx). Estimates are calculated and summed over space and have an r^2 of 0.94.

 https://doi.org/10.1038/s41558-026-02599-9

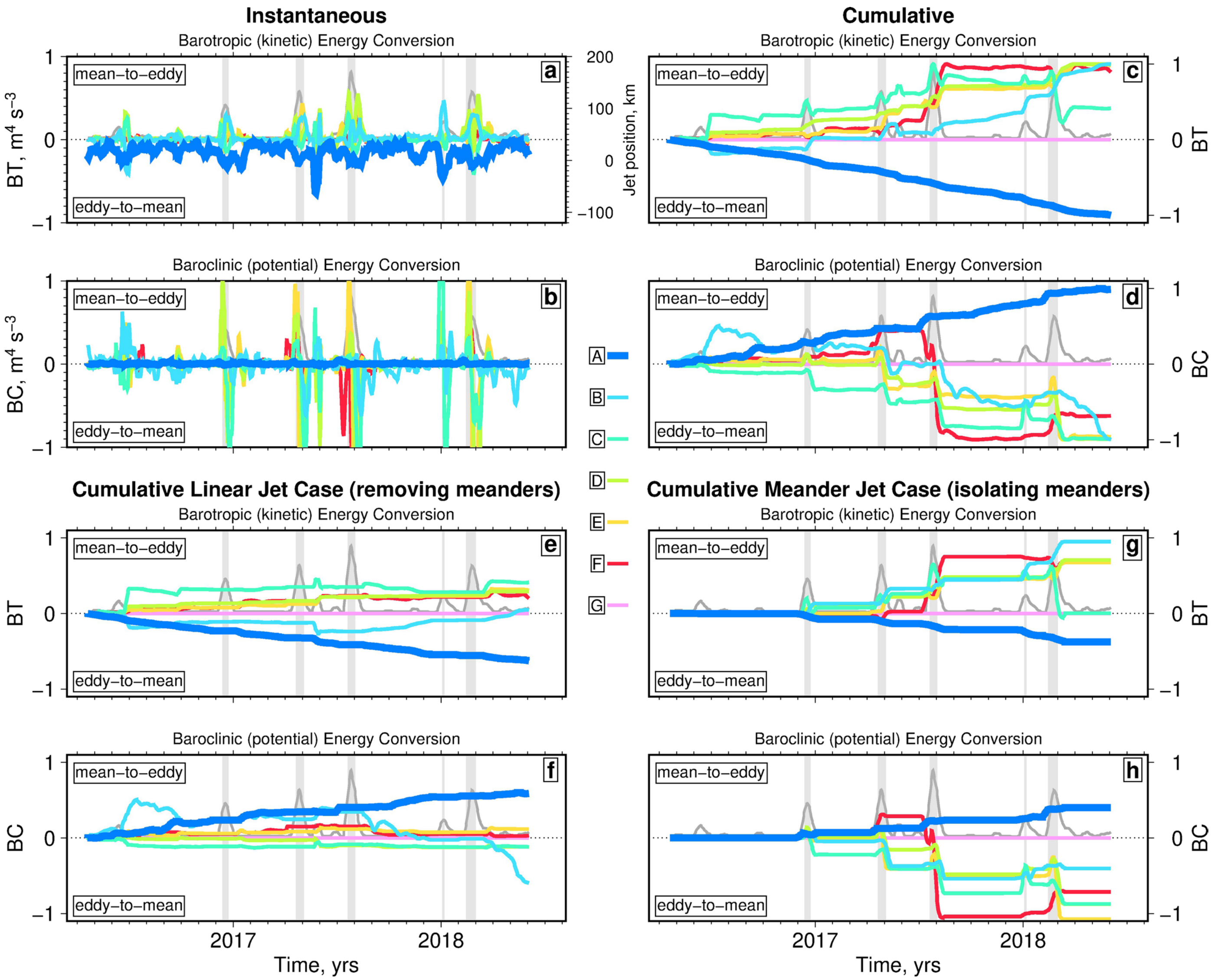

Extended Data Fig. 4 | Instantaneous and overall behavior of energy conversion rates in the Agulhas Current. (**a**,**b**) Time series of depth-integrated barotropic (BT) and baroclinic (BC) energy conversion at each mooring (see key; double thickness line = Mooring A). The largest energy conversion events are strongly correlated with meander periods (grey bars). Positive values indicate mean-to-eddy energy conversion, and vice versa. (**c**,**d**) Temporally-cumulative energy conversion over the deployment period, showing the net role of BT and BC. (**e**-**h**) The same cumulative fluxes partitioned into contributions from the linear (**e**, **f**) and meandering case (**g**, **h**). Energy conversion are normalized by the total (**c**, **d**) to highlight the role and proportional importance of each case.

 https://doi.org/10.1038/s41558-026-02599-9

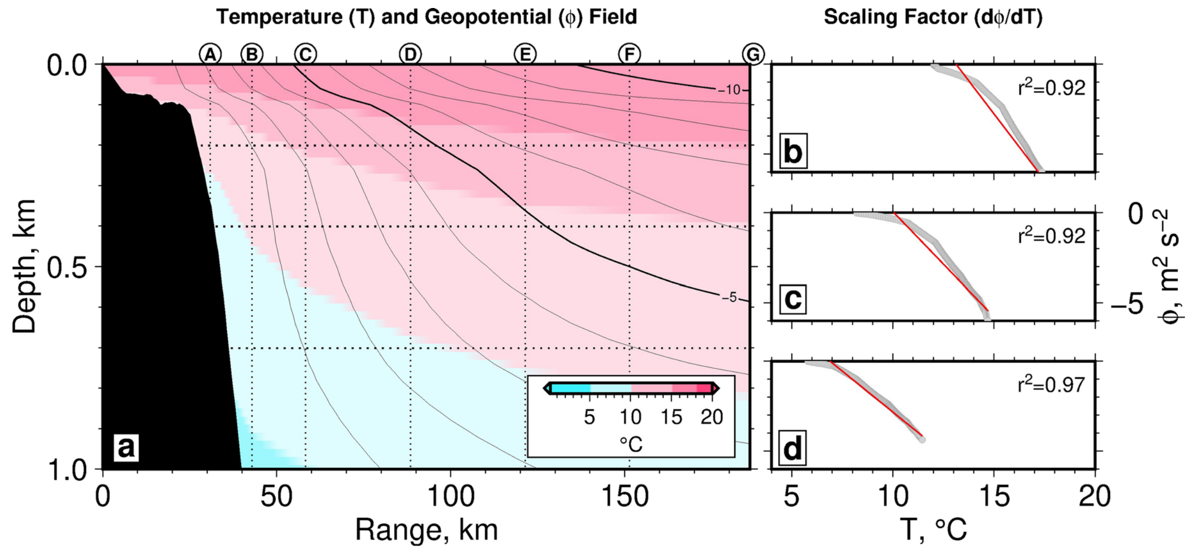

Extended Data Fig. 5 | Strong alignment between streamfunction and temperature. (**a**) Time-mean Conservative Temperature field (T; shading) closely aligned with contours of geopotential anomaly (φ), used here to represent the scaled geostrophic streamfunction (that is $\varphi = f\psi$). (**b**-**d**) The scaling factor between the two fields, dφ/dT, is estimated using a linear fit (red line) to the observed relationship between φ and T (examples for three representative depths along dotted lines in **a**).